



Enhanced Water Pollutant Removal Using Titanium Doped Nickel Ferrite via Photocatalytic Degradation

Eman Z. Hegazy^{*a}, Islam Hamdy Abd El Maksod^a, Shaymaa El-Sayed El-Shafey^a

^a Physical Chemistry Department, National Research Centre (NRC), Cairo 12622, Egypt



Abstract

Nickel ferrite (NiFe₂O₄), known for its magnetic and semiconducting properties, has potential for photocatalytic applications in environmental remediation. This study investigates the effect of titanium (Ti) doping on the structural, morphological, and photocatalytic properties of nickel ferrite. Ti-doped nickel ferrite samples were synthesized using the co-precipitation method and characterized by XRD, SEM, EDX, and UV-Vis spectroscopy. Photocatalytic activity was evaluated through methylene blue (MB) dye degradation under UV light. Optimal Ti doping improved photocatalytic performance, with sample 3 exhibiting a 40% increase and sample 4 achieving up to 90% degradation efficiency. This improvement is attributed to enhanced charge separation and reduced recombination rates due to Ti incorporation. These results suggest that Ti-doped nickel ferrite is a promising, sustainable photocatalyst for water treatment applications. Future work should explore the scalability, cost-effectiveness, and durability of these materials in continuous use.

Keywords: Photocatalysis, Nickel ferrite, Ti doping, Methylene blue degradation, Reactive oxygen species

Introduction

Nickel ferrite (NiFe₂O₄) is a spinel-structured ferrite with a cubic crystal system, where nickel (Ni²⁺) and iron (Fe³⁺) ions occupy the octahedral and tetrahedral sites in the crystal lattice [1-2]. This arrangement results in a unique combination of magnetic and semiconducting properties. Nickel ferrite exhibits a moderate bandgap, typically around 1.5 to 2.0 eV, which is suitable for various photocatalytic applications. Its semiconducting nature allows it to absorb light and generate electron-hole pairs, which are essential for initiating redox reactions on the catalyst surface [3-5]. This makes nickel ferrite an effective photocatalyst for degrading organic pollutants, splitting water to produce hydrogen, and other environmental and energy-related applications [6]. The combination of its magnetic properties with its semiconducting behaviour also enables easy separation and recovery of the catalyst from reaction mixtures using external magnetic fields, enhancing its practicality and efficiency in repeated use [7].

Despite its promising properties, nickel ferrite (NiFe₂O₄) as a photocatalyst faces several limitations, primarily related to its relatively narrow absorption spectrum and high recombination rate of photogenerated electron-hole pairs [8-10]. These factors hinder its overall photocatalytic efficiency. To overcome these limitations, doping nickel ferrite with foreign cations such as titanium dioxide (TiO₂) has been explored. TiO₂ is well-known for its superior photocatalytic activity, wide bandgap, and strong oxidative power. When doped with TiO₂, the composite material can exhibit improved light absorption, reduced electron-hole recombination, and enhanced surface area, leading to increased photocatalytic performance [9-12]. This doping not only extends the absorption spectrum into the visible light range but also stabilizes the structural and electronic properties of nickel ferrite, making the doped material more effective for applications in environmental remediation and renewable energy production.

Methylene Blue (MB) dye is widely used in various industries, including textiles, printing, paper, and medical diagnostics, due to its strong chromatic properties and effectiveness as a staining agent. However, its widespread use leads to significant environmental pollution, as MB is highly soluble in water and resistant to natural degradation processes, posing a threat to

*Corresponding author e-mail: ehgazzy77@yahoo.com; (Eman Z. Hegazy).

Received date 07 October 2024; revised date 31 October 2024; accepted date 04 November 2024

DOI: 10.21608/ejchem.2024.325895.10588

©2025 National Information and Documentation Center (NIDOC)

aquatic life and human health [13-15]. Therefore, there is a critical need to develop effective methods for MB dye removal from wastewater. Photodegradation using catalysts with magnetic properties has emerged as a promising solution. Magnetic photocatalysts, such as those incorporating nickel ferrite, offer the advantage of easy recovery and reuse. After degrading the dye under light exposure, these catalysts can be efficiently separated from the treated water using an external magnetic field, minimizing secondary pollution and operational costs. This approach not only enhances the sustainability of wastewater treatment processes but also ensures the thorough elimination of harmful dye pollutants from the environment [15-17].

In this study, we explore the process of doping titanium into the nickel ferrite catalyst to enhance its photocatalytic activity for the degradation of methylene blue (MB) dye under ultraviolet (UV) irradiation. We delve into the synthesis of the doped catalyst and analyze its structural, morphological, and optical properties. Furthermore, we investigate the photocatalytic performance of the doped nickel ferrite catalyst through a series of UV-induced degradation experiments using MB dye as the model pollutant. By thoroughly examining the efficiency of the doped catalyst in degrading MB dye molecules under UV light exposure, we aim to elucidate its potential as a sustainable and effective solution for environmental remediation applications.

1. Materials & Methods

1.1. Materials

Nickel nitrate ($\text{Ni}(\text{NO}_3)_2 \cdot 6\text{H}_2\text{O}$) (Merck), Iron Nitrate ($\text{Fe}(\text{NO}_3)_3 \cdot 9\text{H}_2\text{O}$) (Merck), Sodium hydroxide (NaOH) (Merck), titanium isopropoxide (Merck) ($d=0.955$). Methylene Blue Dye (Merck)

2.2 Preparation of Nickel ferrite and doped samples:

The preparation process utilized the co-precipitation method with sodium hydroxide as the precipitating agent. Titanium isopropoxide was added during precipitation. The samples were then filtered, dried, and calcined at 700°C for 4 hours. Table 1 outlines the composition of all prepared samples, detailing the sample names and the mole percentage ratios of each constituent element.

Table 1: Elemental Composition of Prepared Mixture

| Sample | Mole % | | |
|----------|--------|-------|-------|
| | Ti | Ni | Fe |
| Sample 0 | 0 | 14.28 | 28.57 |
| Sample 1 | 1.75 | 13.53 | 27.06 |
| Sample 2 | 1.12 | 13.8 | 27.61 |
| Sample 3 | 0.685 | 13.99 | 27.98 |
| Sample 4 | 0.342 | 14 | 28 |

2.3 X-ray powder diffraction analysis (XRD)

X-ray powder diffraction (XRD) analysis was performed to investigate the crystalline phase and crystallite size of the catalyst nanoparticle samples. This analysis utilized a Rigaku X-ray diffractometer system equipped with a RINT 2000 wide-angle goniometer and $\text{Cu K}\alpha$ radiation ($\lambda = 0.15478$ nm) at 40 kV and 30 mA power. Intensity data were collected at room temperature within a 2θ range of 4° to 80° . Additionally, crystal lattice analysis was conducted using accompanying software to calculate deviations in lattice parameters due to Ti incorporation.

2.4 Scanning electron microscopy (SEM)

Scanning electron microscopy (SEM) was used to characterize the morphology of the prepared materials. The obtained micrographs showed the particle morphology (e.g., circular, cubic) of the synthesized materials and identified any amorphous phases present in the samples. The surface morphology and particle shape of all samples were examined using a field emission SEM, specifically the JEOL JSM-7600F system. This SEM is coupled with energy-dispersive X-ray spectroscopy, which allows for composition and elemental analysis, facilitating the examination of ferrite morphological structures and the calculation of surface excess concentrations.

2.5. Surface area measurements (Brunauer Emmett Teller (BET))

The textural characteristics, including BET surface area, pore size distribution, and pore volume, of the samples were determined through N₂-physisorption measurements at -197 °C. A Quantachrome ASiQ automated gas adsorption system was used to obtain N₂ adsorption and desorption data for all samples. Additionally, statistical analysis was conducted to evaluate the pore size distribution.

2.6 Photochemical reactor

The photochemical reactor is equipped with three custom-made UV lamps, each rated at 9 watts and emitting light in the 200-280 nm range (type C). The reactor contains a mixture of 0.1 g of catalyst and 100 mL of 10 PPM Methyl Green dye. Images of the reactor are shown below. Small volume samples are periodically taken for UV analysis.

2.7. DRUV-vis spectral data

Spectral data in the UV-Vis range were acquired using a Jasco V770 UV-Vis spectrometer equipped with an integrating sphere. The measured wavelength range was from 200 to 2000 nm to capture the reflectance spectra of the samples.

3. Results and discussions:

3.1 XRD diffraction:

In Figure 1, the XRD diffraction patterns of all the prepared samples are depicted. It's observed that the undoped sample (Sample 0) exclusively displayed NiFe₂O₄ phases, indicating the absence of any detectable Fe₂O₃ phase according to XRD analysis. However, in the doped samples, a small Fe₂O₃ phase is discernible in addition to the NiFe₂O₄ phases, suggesting the incorporation of Fe₂O₃ into the crystal structure.

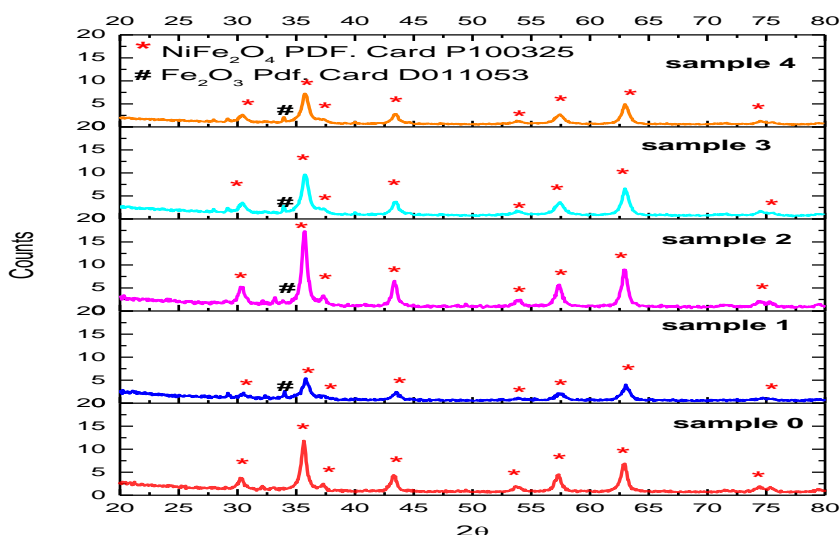


Fig. 1 XRD pattern of all samples under investigations with different Ti doping with phase detection

Table 2. presents the phases, % composition of NiFe₂O₄ and Fe₂O₃, relative degree of crystallinity, and crystallite size (nm) for each sample. The relative degree of crystallinity and the % composition is based on the calculation of area under the max peak of each phase. Supposing that the degree of crystallinity of undoped sample is 100%.

Table 2: XRD composition analysis with crystallite size

| sample | Phases % composition | | Relative degree of crystallinity | Crystallite size (nm) | |
|----------|----------------------------------|--------------------------------|----------------------------------|----------------------------------|--------------------------------|
| | NiFe ₂ O ₄ | Fe ₂ O ₃ | | NiFe ₂ O ₄ | Fe ₂ O ₃ |
| Sample 0 | 100 | 0 | 100 | 31.52 | 0 |
| Sample 1 | 94.1 | 5.6 | 44.6 | 23.5 | 110.6 |
| Sample 2 | 96.5 | 3.5 | 127.7 | 32.4 | 92.17 |
| Sample 3 | 96.3 | 3.7 | 81.13 | 25.05 | 69.13 |
| Sample 4 | 96.2 | 3.8 | 75.2 | 24.3 | 62.1 |

From this table it could be observed that Sample 0 (Undoped) Consists entirely of NiFe₂O₄ with no Fe₂O₃ phase detected. It exhibits a relative degree of crystallinity of 100% with a crystallite size of 31.52 nm. While, sample 1 (Max Ti Doping), Shows a slight increase in the Fe₂O₃ phase (5.6%) compared to the undoped sample. The relative degree of crystallinity decreases to 44.6%, and the crystallite size decreases to 23.5 nm. Sample 2 (Moderate Ti Doping) Maintains a predominantly NiFe₂O₄ phase with a minor increase in Fe₂O₃ (3.5%). It exhibits a higher relative degree of crystallinity (127.7%) and a larger crystallite size (32.4 nm) compared to Sample 1. Moreover, sample 4 (Low Ti Doping) were found to be Similar to Sample 2, with slightly higher Fe₂O₃ content (3.7%). It shows a relative degree of crystallinity of 81.13%, 75% respectively and a crystallite size of 25.05 and 24.3 nm.

The introduction of Ti⁴⁺ ions into the spinel structure hinges largely on the compatibility of ion sizes and the stability of the resulting substitution. This means that Ti⁴⁺ ions, with their ionic radius measuring 0.61 Å, tend to substitute Fe³⁺ ions, which have a similar radius of 0.645 Å, primarily within the octahedral sites of the spinel lattice. This preference arises from their closely matching ionic radii and compatible charge states. As a consequence of this substitution, Fe₂O₃ phases become evident during the doping process.

The incorporation of titanium (Ti) into nickel ferrite exerts a substantial impact on its properties. Yet, the degree of doping, expressed as a percentage, plays a crucial role in determining the material's performance. This influence stems from achieving an optimal balance among various factors, including crystallite size, adsorption capacity, and defect density. Striking this delicate equilibrium enhances both the surface properties and electronic structure of the material, rendering it more conducive to efficient photocatalysis. Later assessments of photocatalytic activity will reveal the tangible effects of this optimization process.

3.2 Diffuse reflectance

DR UV-vis spectral analysis was conducted using the UV-Vis Spectrometer Jasco v770, which was equipped with an integrating sphere to ensure accurate measurements. A comprehensive experimental protocol is delineated in reference [18], providing a detailed account of the procedures followed. The determination of band gap energy values for each sample was accomplished employing the Kubelka-Munk method, a technique previously outlined in our prior research [19].

The Kubelka-Munk factor (K) was computed utilizing the formula:

$$K = (1 - R)^2 / 2R$$

where R denotes the percentage reflectance. Subsequently, wavelengths (nm) were converted into energies (E), facilitating the plotting of a graph between $(K * E)^{0.5}$ and E. The bandgap energy (eV) was pinpointed at the intersection of the two slopes on this curve.

Fig. (2) presents the resultant curves and band gap values for all samples under scrutiny. Notably, the band gap values fall within the range typical of Nickel ferrite materials (1.5-2) [20]. It is essential to highlight that the introduction of titanium into the lattice structure of ferrite materials leads to a minor adjustment in these values, tending toward larger magnitudes.

It's apparent from the observed curve that the band gap values display an indirect correlation with preceding parameters, such as crystallite size or even the degree of crystallinity. This observation underscores the complexity of the situation, where multiple factors contribute to determining the band gap value. Nevertheless, the notable increase in band gap at the lowest level of titanium doping may hint at its distinctive characteristics, which will be further elucidated through photocatalytic activity analysis.

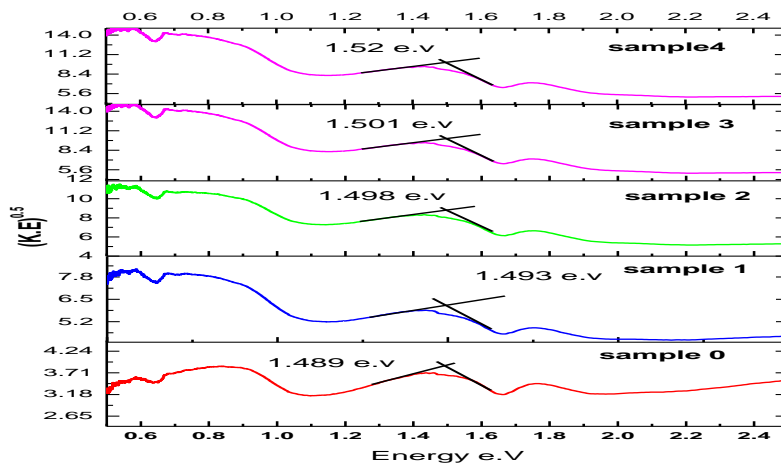


Fig. 2 Kubelka-Munk figures employed for the calculation of band gap values.

3.3 SEM Images:

The scanning electron microscopy (SEM) analysis of the Nickel ferrite samples revealed detailed insights into their structural characteristics. The SEM images showcased distinct crystal structures of ferrite across all samples. However, a significant difference was observed in the Ti-doped samples compared to the undoped ones. The Ti-doped samples exhibited a more porous and fluffy appearance, suggesting that the introduction of Ti into the ferrite lattice induced alterations in the material's porous structure. These structural changes imply that Ti doping affects the overall morphology of the ferrite samples. The subsequent surface analysis section will further explore and elucidate these findings, providing a deeper understanding of the impact of Ti doping on the properties and behaviour of the ferrite samples

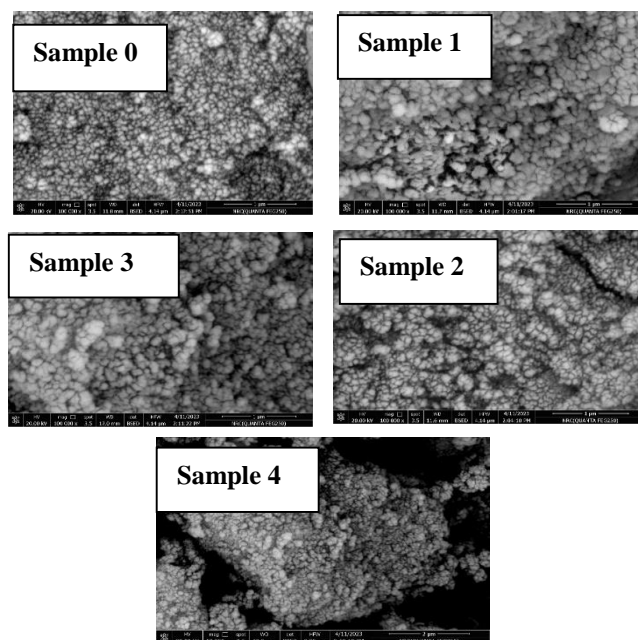


Fig. 3 SEM images of all prepared samples

3.4 EDX Analysis of the prepared samples

The Energy Dispersive X-ray (EDX) analysis provided detailed compositional data for the samples, summarized in the table (3) below:

The EDX analysis indicates the following key points:

- Sample 0 has no Ti present.
- Sample 1 has the highest Ti content with 3.33 atomic %, and the lowest O/Ti ratio (19.70).
- Sample 2 has moderate Ti content (0.60 atomic %) with an intermediate O/Ti ratio (98.06).
- Sample 3 has lower Ti content (0.45 atomic %) but the higher O/Ti ratio (147.07).
- Sample 4 has the lowest Ti content (0.17) but the highest O/Ti ratio (400)

Table 3: EDX analysis of samples under investigation

| sample | atomic % | | | | O/Ti |
|--------|----------|-------|-------|------|----------|
| | Ni | Fe | O | Ti | |
| 0 | 13.29 | 27.97 | 58.74 | 0.00 | |
| 1 | 9.93 | 21.06 | 65.67 | 3.33 | 19.69547 |
| 2 | 13.39 | 27.41 | 58.61 | 0.60 | 98.0625 |
| 3 | 10.34 | 22.81 | 66.40 | 0.45 | 147.0667 |
| 4 | 9.00 | 23.00 | 68.00 | 0.17 | 400 |

The high O/Ti ratio in Samples 3 (147.07) and sample 4 (400) might indicate a more favorable oxidation state or surface chemistry for photocatalytic activity. A high oxygen content relative to titanium could enhance the formation of active sites necessary for photodegradation processes. Additionally, as suggested by SEM analysis, Ti-doped samples, especially Sample 3, exhibit a more porous and fluffy structure. This increased porosity can enhance the surface area available for photocatalytic reactions, thereby improving efficiency.

Therefore, based on the EDX data, it can be inferred that the structural and compositional properties, especially the O/Ti ratio and the porous nature induced by Ti doping, play a significant role in enhancing the photocatalytic activity of Sample 3 and 4. Further detailed analysis of surface states and electronic properties, as will be seen in the next section, could provide deeper insights into these observations.

3.5 Photo catalytic degradation of Methylene blue:

Figure 4 presents the photocatalytic degradation curves of all investigated samples under UV irradiation. The results indicate that samples 0, 1, and 2 exhibited very low catalytic activity, achieving only 1-5% degradation. In contrast, a significant change was observed in the samples with very low Ti doping (samples 3 and 4). Specifically, sample 3 showed a dramatic increase in degradation efficiency, reaching approximately 40% increase, and sample 4 exhibited another non-linear increase in degradation efficiency to be around 90%.

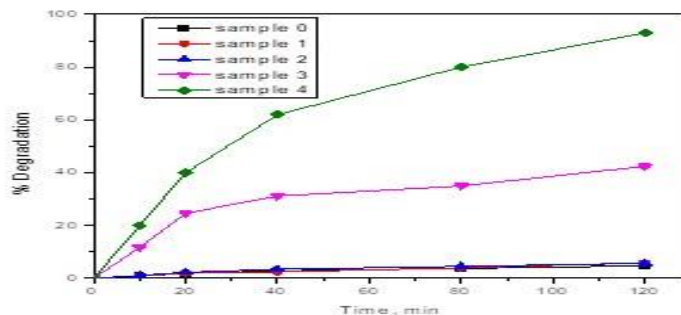


Fig. 4 Photo degradation curves under UV Irradiation of all investigated samples

These findings suggest that Ti doping at critical concentrations induces substantial changes in the surface and catalytic behavior of nickel ferrite samples. Although sample 1 has the highest Ti content, its photodegradation efficiency is much lower compared to samples 3 and 4. This implies that an optimal Ti doping level, rather than the maximum possible, is crucial for enhancing photocatalytic efficiency. Excessive Ti doping may introduce recombination centers that reduce the photocatalytic performance.

Table (4) showed the adsorption capacity of all samples compared with measured BET surface area. The results demonstrate the favorable impact of titanium (Ti) doping on the adsorption capacity and BET surface area of nickel ferrite catalysts for methylene blue (MB) dye removal. A clear increasing trend in both adsorption capacity and surface area is observed with increasing Ti doping levels, indicating the crucial role of Ti in enhancing the surface properties of the catalyst. Samples with higher Ti doping levels, particularly Sample 3 and Sample 4, exhibit significantly higher adsorption capacities and surface areas, suggesting their potential for efficient MB dye removal from wastewater. These findings underscore the importance of optimizing Ti doping levels to enhance the performance of nickel ferrite catalysts for environmental remediation applications. However, the relationship between adsorption capacity, surface area, and photocatalytic activity are much more complicated.

Table 4: comparison of adsorption capacity with BET surface area

| sample | Adsorption capacity (mg/g) | BET surface area (m ² /g) |
|----------|----------------------------|--------------------------------------|
| Sample 0 | 0.6 | 15 |
| Sample 1 | 1.05 | 20 |
| Sample 2 | 2.20 | 25 |
| Sample 3 | 2.27 | 26 |
| Sample 4 | 2.5 | 27 |

This behavior is further corroborated by the Energy Dispersive X-ray (EDX) analysis results (Table 3). The O/Ti ratio in sample 3 was about 147, whereas in sample 4, by reducing the Ti doping to nearly half that of sample 3, the O/Ti ratio doubled. This increase in the O/Ti ratio was accompanied by a doubling of the photocatalytic activity. These observations highlight the importance of optimizing the Ti doping level to achieve maximum photocatalytic efficiency in nickel ferrite samples.

Table (5) provides a comparative analysis of the photocatalytic activity of Ti-doped nickel ferrite from our study with similar catalysts reported in the literature. Our Ti-doped nickel ferrite demonstrates superior performance, achieving up to 90% methylene blue degradation under UV light, surpassing other doped ferrite systems like Ti-doped ferrites by Ganesh et al. (2023) [Ref. 15] and Arumugham et al. (2022) [Ref. 9], which reported degradation efficiencies of around 70-80%.

Table 5: comparison between our study and previous studies

| Reference | Catalyst | Photocatalytic Activity (Degradation Efficiency) |
|---|------------------------------------|--|
| our Study | Ti-doped Nickel Ferrite | Up to 90% degradation of methylene blue under UV light |
| Ganesh et al. (2023) [Ref. 15] | Ti-doped Nickel Ferrite | ~70% degradation of organic dyes under visible light |
| Arumugham et al. (2022) [Ref. 9] | Ti-doped Nickel Ferrite composites | >80% degradation of dyes under visible light |

3.6. Suggested Mechanism for Degradation of Methylene Blue (MB) over Ti-Doped Nickel Ferrite Catalyst:

The degradation of methylene blue (MB) over the Ti-doped nickel ferrite catalyst involves several key steps, including light absorption, electron-hole pair generation, charge separation, and subsequent redox reactions. Here's a detailed mechanism explaining the process:

1. Light Absorption:

Upon exposure to UV light, the Ti-doped nickel ferrite catalyst absorbs photons with energy equal to or greater than its band gap energy. The band gap of nickel ferrite is typically around 1.5 to 2.0 eV, and doping with titanium (Ti) can slightly alter this value, enhancing light absorption properties.

2. Generation of Electron-Hole Pairs:

The absorbed photons excite electrons (e^-) from the valence band (VB) to the conduction band (CB), leaving behind holes (h^+) in the VB:



3. Charge Separation:

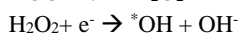
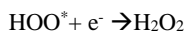
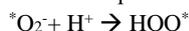
The presence of Ti doping helps in reducing the recombination rate of electron-hole pairs. Ti^{4+} ions substitute Fe^{3+} ions in the ferrite structure, which can create localized energy states that facilitate better charge separation and migration of electrons and holes to the surface of the catalyst.

4. Generation of Reactive Oxygen Species (ROS):

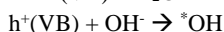
The photogenerated electrons (e^-) in the conduction band can reduce molecular oxygen (O_2) adsorbed on the catalyst surface to form superoxide anions ($\bullet\text{O}_2^-$):



These superoxide anions can further react to form hydrogen peroxide (H_2O_2) and hydroxyl radicals ($\bullet\text{OH}$):



Simultaneously, the holes (h^+) in the valence band can directly oxidize water (H_2O) or hydroxide ions (OH^-) to produce hydroxyl radicals ($\bullet\text{OH}$):



5. Degradation of Methylene Blue (MB):

The generated reactive oxygen species (ROS), particularly hydroxyl radicals ($\bullet\text{OH}$) and superoxide anions ($\bullet\text{O}_2^-$), are highly reactive and can attack the MB dye molecules, leading to their degradation through various oxidative pathways:



These oxidative reactions break down the chromophore structure of MB, leading to decolorization and mineralization into smaller, less harmful molecules such as CO_2 , H_2O , and inorganic salts.

The proposed mechanism highlights the critical role of Ti doping in enhancing the photocatalytic efficiency of nickel ferrite by improving charge separation and increasing the generation of reactive oxygen species. These ROS play a vital role in the oxidative degradation of methylene blue, leading to effective removal of the dye from aqueous solutions. This mechanism provides valuable insights into the photocatalytic process and the potential for optimizing nickel ferrite-based catalysts for environmental remediation applications.

4. Conclusions:

This study demonstrates that titanium (Ti) doping significantly enhances the photocatalytic performance of nickel ferrite (NiFe_2O_4). X-ray diffraction (XRD) analysis confirmed the presence of NiFe_2O_4 phases alongside minor Fe_2O_3 inclusions

following Ti doping. Scanning electron microscopy (SEM) images showed increased porosity and a fluffier texture in the Ti-doped samples, indicating structural changes. Energy-dispersive X-ray spectroscopy (EDX) analysis revealed a critical correlation between the oxygen-to-titanium (O/Ti) ratio and photocatalytic efficiency.

The samples with optimal Ti concentrations (Samples 3 and 4) demonstrated the highest photocatalytic activity, achieving 40% and 90% degradation of methylene blue dye, respectively. These findings underscore the importance of carefully optimizing Ti doping levels to enhance the photocatalytic efficiency of nickel ferrite. However, it is crucial to note that excessive Ti doping can introduce recombination centers that diminish overall performance. Therefore, maintaining an optimal Ti concentration is essential for maximizing the photocatalytic properties of this material, ensuring effective degradation of pollutants in practical applications.

5. References:

1. Fariba Kaedi, Zahra Yavari, Ahmad Reza Abbasian, Milad Asmaei, Kagan Kerman, Meissam Noroozifar. "Synergistic influence of mesoporous spinel nickel ferrite on the electrocatalytic activity of nano-structured palladium." **RSC Advances**, Volume 11, Issue 20, 2021, Pages 11813-11820. DOI: 10.1039/d0ra10944d.
2. P. Annie Vinosha, A. Manikandan, R. Ragu, A. Dinesh, K. Thanrasu, Y. Slimani, A. Baykal, Belina Xavier. "Impact of nickel substitution on structure, magneto-optical, electrical and acoustical properties of cobalt ferrite nanoparticles." **Journal of Alloys and Compounds**, Volume 857, 2021, 157517. DOI: 10.1016/j.jallcom.2020.157517.
3. M. Ounacer, B. Rabi, E. Agouriane, A. Essoumhi, M. Sajieddine, B.F.O. Costa. "Structural, magnetic, and Mössbauer studies of magnetite and nickel-copper and nickel-zinc ferrites." **Inorganic Chemistry Communications**, Volume 158, Part 2, 2023, 111650. DOI: 10.1016/j.inoche.2023.111650.
4. Anju Ganesh, Sherin Sara Philip, Nowfina Kabeer, Smitha Thankachan, Nayomi John, G. Hrishikesh, Aleena Sebastian. "Photocatalytic and anti-bacterial application of nickel ferrites synthesised from microwave method." **Materials Today: Proceedings**, 2023. DOI: 10.1016/j.matpr.2023.11.099.
5. Rosane S. Melo, Adolfo Franco, Prasun Banerjee. "Nanoscale-driven single-domain structure in nickel substituted superparamagnetic cobalt ferrites." **Solid State Communications**, Volume 341, 2022, 114560. DOI: 10.1016/j.ssc.2021.114560.
6. Jitao Zhang, Xingkui Mu, Qingfang Zhang, Natallia Poddubnaya, Dmitry Filippov, Jiagui Tao, Fang Wang, Liying Jiang, Lingzhi Cao. "Structural, micro-structure, magnetic and dynamic magneto-elastic properties of samarium-doped nickel-zinc spinel ferrites for efficient power conversion applications." **Journal of Magnetism and Magnetic Materials**, Volume 602, 2024, 172176. DOI: 10.1016/j.jmmm.2024.172176.
7. Yu-jia Sun, Yi-fei Diao, Hui-gang Wang, Guangju Chen, Mei Zhang, Min Guo. "Synthesis, structure and magnetic properties of spinel ferrite (Ni, Cu, Co)Fe₂O₄ from low nickel matte." **Ceramics International**, Volume 43, Issue 18, 2017, Pages 16474-16481. DOI: 10.1016/j.ceramint.2017.09.029.
8. Pan Xiong, Yongsheng Fu, Lianjun Wang, Xin Wang. "Multi-walled carbon nanotubes supported nickel ferrite: A magnetically recyclable photocatalyst with high photocatalytic activity on degradation of phenols." **Chemical Engineering Journal**, Volumes 195–196, 2012, Pages 149-157. DOI: 10.1016/j.cej.2012.05.007.
9. Nagaveni Arumugham, Anusuya Mariappan, Jayanthi Eswaran, Santhanaraj Daniel, Rajakumar Kanthapazham, Poonkodi Kathirvel. "Nickel ferrite-based composites and its photocatalytic application – A review." **Journal of Hazardous Materials Advances**, Volume 8, 2022, 100156. DOI: 10.1016/j.hazadv.2022.100156.
10. Nehad Ahmed Hassan Mohammed, Rehab Nabil Shamma, Sherien Elagroudy, Adewale Adewuyi. "Chitosan incorporated nickel ferrite photocatalyst for complete photocatalytic degradation of ciprofloxacin, ampicillin and erythromycin in water." **Results in Chemistry**, Volume 7, 2024, 101307. DOI: 10.1016/j.rechem.2024.101307.
11. O. Rosales-González, A.M. Bolarín-Miró, C.A. Cortés-Escobedo, F. Pedro-García, J.A. Patiño-Pineda, F. Sánchez-De Jesús. "Synthesis of a magnetically removable visible-light photocatalyst based on nickel-doped zinc ferrite." **Ceramics International**, Volume 49, Issue 4, 2023, Pages 6006-6014. DOI: 10.1016/j.ceramint.2022.10.101.

12. Charanjit Singh, S. Bansal, Vinod Kumar, Sonal Singhal. "Beading of cobalt substituted nickel ferrite nanoparticles on the surface of carbon nanotubes: a study of their synthesis mechanism, structure, magnetic, optical and their application as photocatalyst." **Ceramics International**, Volume 41, Issue 3, Part A, 2015, Pages 3595-3604. DOI: 10.1016/j.ceramint.2014.11.021.
13. Saravanan Selvaraj, D. Simon Patrick, V.S. Manikandan, Govind A Vangari, M. Krishna Mohan, M. Navaneethan. "Synergistic effects of La-doping on ZnO nanostructured photocatalysts for enhanced MB dye degradation." **Surfaces and Interfaces**, 2024, 104538. DOI: 10.1016/j.surfin.2024.104538.
14. Kheira Chinoune, Amel Mekki, Bouhadjar Boukoussa, Adel Mokhtar, Amina Sardi, Mohammed Hachemaoui, Jibrán Iqbal, Issam Ismail, Mohamed Abboud, Wael A. Aboneama. "Adsorption behavior of MB dye on alginate-sepiolite biocomposite beads: Adsorption, kinetics, and modeling." **Inorganic Chemistry Communications**, Volume 165, 2024, 112558. DOI: 10.1016/j.inoche.2024.112558.
15. P.S. Nandisha, Sowbhagya, G. Vinay. "One-step facile combustion synthesis of dual-phased Mn₃O₄- γ -MnS nanocomposite for photodegradation of Methylene blue (MB) dye." **Materials Letters**, Volume 360, 2024, 135963. DOI: 10.1016/j.matlet.2024.135963.
16. Swarnima Athavale, Divya P. Barai, Bharat A. Bhanvase, Shekhar L. Pandharipande. "Investigation on performance of Eu:GO:K₂SrPO₄ nanocomposite for MB dye photocatalytic degradation: Experimental and ANN modeling." **Optik**, Volume 275, 2023, 170561. DOI: 10.1016/j.ijleo.2023.170561.
17. Prafulla Kumar Panda, Rasmirekha Pattanaik, Saswati Mishra, Debapriya Pradhan, Suresh Kumar Dash. "Superior photocatalytic degradation of MB dye using BiVO₄ nanoparticles under solar light irradiation." **Materials Today: Proceedings**, 2023. DOI: 10.1016/j.matpr.2023.11.039.
18. Bing Sun, Fugang Chen, Wenda Yang, Hongqing Shen, Dan Xie. "Effects of nano-TiO₂ and normal size TiO₂ additions on the microstructure and magnetic properties of manganese-zinc power ferrites." **Journal of Magnetism and Magnetic Materials**, Volume 349, 2014, Pages 180-187.
19. Islam Hamdy Abd El Maksod, Abdelmohsen Al-Shehri, Salem Bawaked, Mohamed Mokhtar, Katabathini Narasimharao. "Structural and photocatalytic properties of precious metals modified TiO₂-BEA zeolite composites." **Molecular Catalysis**, Volume 441, 2017, Pages 140-149.
20. Anju Ganesh, Manju Kurian, Nayomi John, Smitha Thankachan. "Structural and magnetic properties of sol-gel autocombustion and microwave synthesized nickel ferrite nanoparticles and their photocatalytic and anti-microbial applications." **Materials Today: Proceedings**, 2023. DOI: 10.1016/j.matpr.2023.11.118.